

Simulation of a Zenith-Field Sky Survey on RATAN-600

E.K. Majorova¹

Special Astrophysical Observatory Russian Academy of Sciences, N. Arkhyz, KChR, 369167, Russia

Received: November 1, 2007/Revised: November 29, 2007

Abstract. In this paper we simulate a deep multi-frequency zenith-field sky survey on RATAN-600 (the RZF survey). In our simulations we use the 1.4-GHz sky images obtained in the NVSS survey. We convolved NVSS images with the two-dimensional power beam pattern of RATAN-600 and obtain simulated 24-hour scans of sky transits at all wavelengths of the RZF survey. For the 7.6-cm wavelength we analyze the effect of the image area size on the results of the simulation. We estimate the accuracy of the determination of source fluxes on simulated scans and derive the distributions of the spectral indices of the sources. We use the simulated scans to clean real records of the RZF survey at 7.6 cm. The standard error of the residual noise at this wavelength is about 1 mJy.

1. INTRODUCTION

Sky surveys are among the main sources of information about cosmic objects. The first deep sky survey on RATAN-600 was carried out in 1980–1982 during the “Cold” experiment at the declination of $\delta \sim 5^\circ$ [1]. The use of the best radiometer in terms of fluctuation sensitivity made it possible to obtain new constraints on the background radiation of the Universe and prepare a catalog of radio sources with a detection threshold of ~ 10 mJy (RC catalog) at 7.6 cm [2, 3].

During the period from 1979 through 1987 the multi-frequency “Zelenchuk Survey” in the declination interval $\delta = 0^\circ \div 14^\circ$ [4, 5], and during the period from 1987 through 1989, a polar survey [6], were carried out on the Southern sector with a periscopic reflector. The threshold of 3.9-GHz source detection flux was equal to 50 and 14 mJy for the “Zelenchuk” and polar surveys, respectively. In 1988 the sky area $\delta = 47^\circ 06' 45'' \div 47^\circ 07' 45''$, $8^h \leq \alpha < 14^h$ was observed with the whole ring aperture of RATAN-600 with a detection threshold of ~ 15 mJy [7].

The next step in conducting surveys on RATAN-600 was taken in the late 1990ies. The upgrade of the radio telescope and substantial improvement of the radiometer sensitivity made it possible to perform a deeper survey at a higher quality level.

The RZF survey (RATAN-600 Zenith Field) was performed during the period from 1998 through 2003 on the Northern sector at wavelengths $1.0 \div 55$ cm at declination of 384 . At the main wavelength of observations ($\lambda 7.6$ cm) the half-power survey width was $\delta_{2000.0} = 41^\circ 30' 42'' \pm 2'$, $0^h \leq \alpha_{2000.0} < 24^h$. As a result of the survey, a catalog of

radio sources at 7.6 cm (the RZF catalog) was compiled [8]. The minimum flux of the radio sources of the RZF catalog was close to about 2.5 mJy, which is comparable to the threshold flux of the NVSS catalog [9]. Starting from 2001, eight sky bands were observed in addition to the central band. The additional bands were shifted by $\Delta\delta = \pm 12'n$ ($n=1, 2, 3, 4$) with respect to the central band. Note that the density of the survey bands in declination was increased by a factor of two since 2006, and the interval between the neighboring bands became equal to $6'$.

A distinctive feature of the sky surveys performed with RATAN-600 compared, e.g., to VLA surveys (NVSS [9], FIRST [10]), is that at a given declination we observe sources located within a certain interval (band) of declinations. The angular size of this band is determined by the size of the vertical power beam (PB) of the radio telescope. The only exception is the sky survey performed in 1988 in the mode of whole circular aperture of the antenna with a “pencil-shaped” beam of the radio telescope at the half-power level. In all other surveys one of the sectors of RATAN-600 was used ($1/4$ of the ring aperture). In this mode of operation the power beam pattern of the radio telescope differs substantially from that of a paraboloid.

A distinctive feature of the power beam of RATAN-600 operating in a single-sector mode is its large extension in the vertical plane and the extended “fan-shaped” background at large elevations, whose intensity decreases as $1/y$ in the vertical plane [11, 12]. Figure 1 gives an example of a PB computed for the elevation angle $H = 88^\circ 42''$. Such a structure of the power beam allows, on the one hand, sources to be observed within a certain declination band and, on the other hand, makes the sources difficult to distinguish and thus results in extended structures ap-

Send offprint requests to: E.K.Majorova, e-mail: len@sao.ru

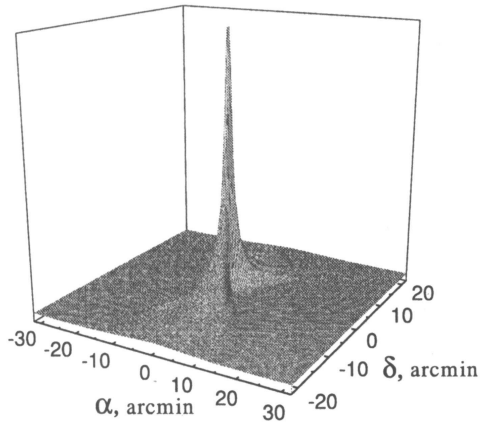


Fig. 1. Power beam pattern of RATAN-600 computed for the wavelength and elevation of 7.6 cm and $H = 88^{\circ}42''$, respectively.

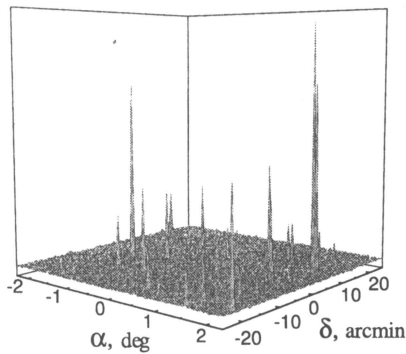


Fig. 2. Fragment of the $4^{\circ} \times 4^{\circ}$ NVSS image. The size in declination is trimmed ($\delta = \pm 20'$).

pearing on the records of sky transits across the fixed PB of the telescope (the so-called sky scans). This is because the magnitude and shape of the signal from an individual source depend substantially on the distance of the source from the central section of the power beam pattern.

In view of the aforesaid, simulation of sky surveys conducted with RATAN-600 is of considerable practical interest. Such simulations are necessary both for studies of extended cosmic objects in order to estimate the contribution of point sources to their flux, and for extraction of numerous weak sources against noise background, thereby reducing the effect of “confusion”.

In this paper we attempt to simulate the RZF sky survey in its central section $\delta_0 = 41^{\circ}30'42''$ using the 1.4-GHz sky images (charts) obtained as a result of the NVSS (NRAO VLA Sky Survey) [9].

2. TECHNIQUE OF SIMULATION OF THE ZENITH-FIELD SURVEY

Bursov and Majorova [13] were the first to simulate the zenith-field sky survey (RZF-survey). To this end,

the above authors used the data of the NVSS catalog, from which they adopted the principal parameters of the sources. The program package for computing the two-dimensional PB of RATAN-600 [11] was used to simulate the curves of the transit of sources across various horizontal sections of the power beam pattern. These computations assumed all sources to be points, i.e., their angular sizes were assumed to be much smaller than the halfwidth of the power beam (HPBW). In this case, the response of the antenna to the transit of a source with declination δ_{ist} across the power beam of the radio telescope is identical to the horizontal section of the power beam shifted by $\Delta\delta$ from the central section and multiplied by the 7.6-cm flux of the source in question. Here $\Delta\delta = \delta_{ist} - \delta_0$, where δ_0 is the declination of the central section of the RZF survey, which passed through 384.

We computed the transit curves for most of the sources of the NVSS catalog, whose declinations fall within the $\Delta\delta = 41^{\circ}30'42'' \pm 30'$ band. To compute the 7.6-cm fluxes of the sources, we used their 21-cm fluxes adopted from the NVSS catalog and the spectral indices of the corresponding sources. For the sources with unavailable spectral indices we set the spectral index equal to $\gamma = -0.8$, which corresponds to a normal nonthermal spectrum ($S_{\nu} \sim \nu^{\gamma}$). We then time shifted the curves in accordance with the right ascension (α) of each particular source, and summed them up. The resulting one-dimensional scan of the diurnal transit of the sky band across the fixed PB of the radio telescope provided a good analog of real observations. Let us refer this model of the RZF-survey as the model based on the NVSS catalog.

In this paper we simulate the zenith-field survey by convolving the two-dimensional PB of RATAN-600 with the VLA NVSS sky images with a resolution of $\theta = 45''$, which have the form of $4^{\circ} \times 4^{\circ}$ areas. The images are in the FITS format and they are available from the NRAO site [14]. Each of the 2326 1024×1034 images has a name in the form PHHMMSDD, where P is the name of the Stokes parameter (I, Q, or U); and MM are the hours and minutes of right ascension of the image center; S, the sign of the declination (P and M for + and -, respectively), and DD is the declination of the image center in degrees for the epoch of 2000 (J2000).

To simulate the RZF survey, we use about 20^m -long intensity images Ihh00PDD, Ihh20PDD, and Ihh40PDD (where $hh = 00, 01, \dots, 23$) with the central declination of $\delta_0 = +40^{\circ}$ for the simulation at $\lambda \leq 7.6$ cm; $\delta_0 = +40^{\circ}$ and $+44^{\circ}$ for the simulation at $\lambda 13$ and 31 cm, and $\delta_0 = +36^{\circ}$, $+40^{\circ}$, and $+44^{\circ}$ for the simulation at $\lambda 49$ cm.

We compute the two-dimensional power beam pattern of RATAN-600 as described by Majorova [11]. We performed our computations for the elevation of 3C84 ($H = 88^{\circ}42''$) in such declination intervals that maximum values of the power beam in the most distant sections are equal to a fraction of percent of the maximum of the diagram in its central section. The width of this declination interval was equal to $d\delta = \pm 6'$, $d\delta = \pm 37'15''$, and $d\delta = \pm 4^{\circ}53'$ for $\lambda 1.0$, $\lambda 7.6$, and $\lambda 49$, respectively. We com-

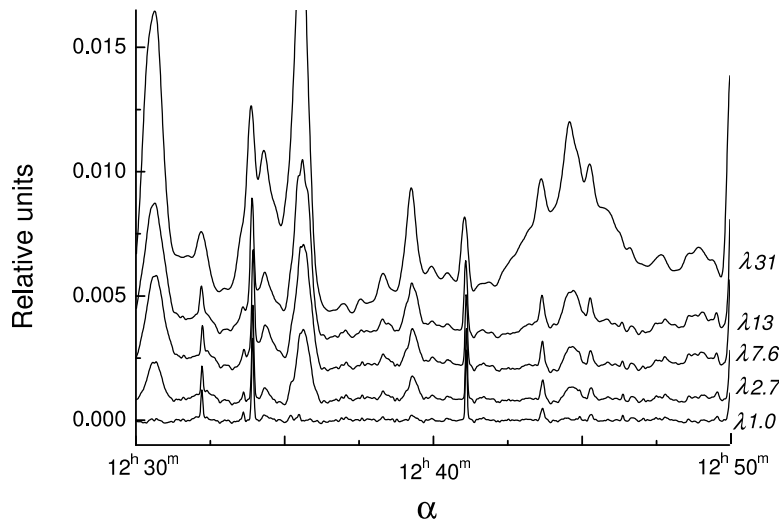


Fig. 3. Normalized simulated 20-minute scans of the $\delta_{2000.0} = 41^{\circ}30'42''$, $12^h30^m \leq \alpha_{2000.0} \leq 12^h50^m$ sky area at wavelengths 1.0, 2.7, 7.6, 13, and 31 cm obtained by convolving the PB of RATAN-600 with the $4^{\circ} \times 4^{\circ}$ areas of NVSS images. We normalized the scans to the signal level from 384. The curves are shifted only along the vertical axis.

pute the power beam pattern of the radio telescope with a step equal to the pixel size on the NVSS survey maps (15 arcsec). Figure 1 shows the two-dimensional power beam computed for the wavelength of 7.6 cm and elevation of $H = 88^{\circ}42''$. The size of the power beam in the figure is trimmed, $d\delta = \pm 20'$.

We convolved the diagram with the part of the NVSS-survey images whose declination size is equal to the vertical size of the computed PB for the corresponding wavelength ($d\delta$). The center of NVSS images was located at the declination of $\delta = 41^{\circ}30'45''$, which virtually coincides with the declination of 384. In addition to the IHHMMP40 images we used IHHMMP44 (at wavelengths 7.6 cm $\lambda_{\lambda}49$ cm) and IHHMMP36 and IHHMMP44 (at the 49-cm wavelength) images. Figure 2 shows an example of an NVSS image with a declination size of $d\delta = \pm 20'$.

We convert the images from the FITS format into binary matrices, which we then convolved with two-dimensional PB. As a result of these convolutions, we obtain 72 one-dimensional 20-minute sky scans at each wavelength. Note that the declination size of NVSS images (and that of the power beam) exceed the width of the survey band at the wavelength considered by more than one order of magnitude, thereby allowing better account to be taken of strong distant sources falling within the PB of the radio telescope. Further increase of image sizes in δ has virtually no effect on the results of the simulation.

We normalize the resulting scans to the level of the 3C84 signal and convert them into F-format files. F format is a modification of FITS format used on RATAN-600 for representing the actual records and for their subsequent reduction.

Figure 3 shows the normalized simulated 20-minute scans of the $\delta_{2000.0} = 41^{\circ}30'42''$, $12^h30^m \leq \alpha_{2000.0} \leq$

12^h50^m sky area at 1.0, 2.7, 7.6, 13, and 31 cm wavelengths obtained using the technique described above. Here and in subsequent figures scans are shifted with respect to each other along the vertical axis for better visualization.

It is evident from the curves presented that as we pass from $\lambda 1.0$ cm to longer wavelengths the halfwidths of the sources in records increase and new sources and extended structures appear. This is due to the increase of the size of the PB with increasing wavelength, so that the power beam begins to cover the sky areas increasingly distant from the central section. Strong sources passing far from the central section in terms of δ would produce extended features similar to the one we see in Fig. 3 at $\lambda 13$ and 31 cm in the right-ascension interval $12^h42^m < \alpha < 12^h47^m$.

Figure 4 shows normalized simulated scans at 7.6, 13, and 31 cm (curves 1) and the corresponding normalized transit curves obtained within the framework of the RZF survey (curves 2). The real records shown in the figures were kindly provided by N. N. Bursov. They were obtained by averaging about 200 transits of the same sky area in the central band of the survey during the period from 1998 through 2003 [16]. The simulated and real scans are normalized to the level of the signal from 384.

The subsequent analysis is based on the results of the simulation of the RZF survey at 7.6 cm. The sensitivity of the RZF survey is maximum at this wavelength and it is close to the sensitivity of the NVSS survey.

It is of interest to compare the results of simulations not only with real records, but also with simulated scans based on the NVSS catalog [13] data. Figure 5 features 20-minute simulated sky scans obtained using NVSS images (curves 1) and simulated scans based on the data of the NVSS catalog (curves 2), as well as the corresponding

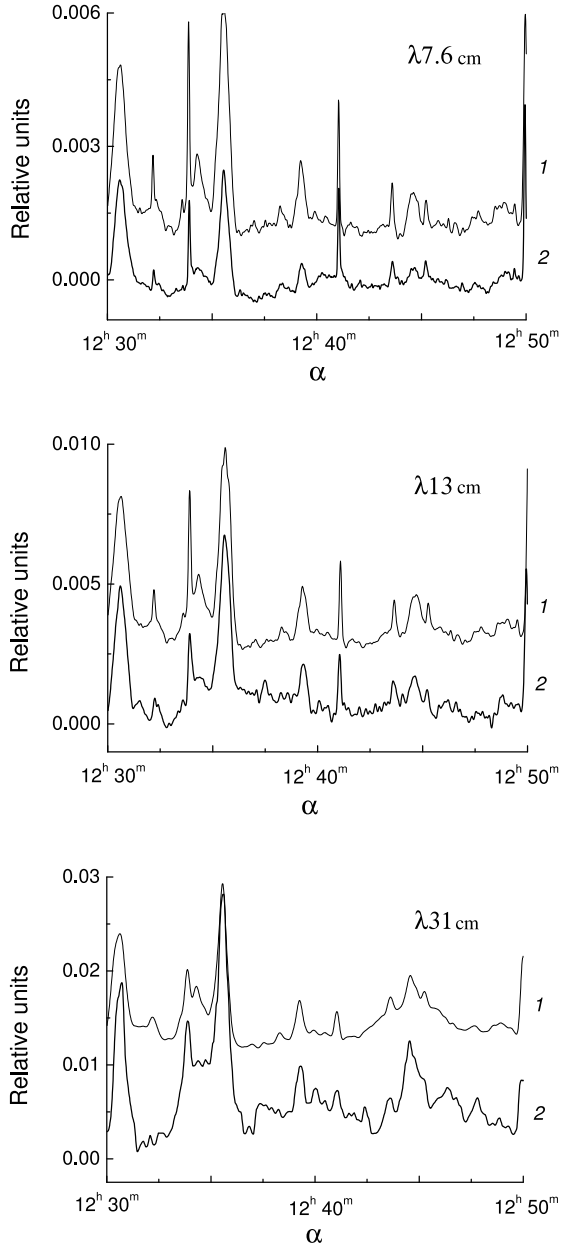


Fig. 4. Normalized simulated scans at the wavelengths of 7.6, 13, and 31 cm obtained using NVSS images (curves 1), and normalized real averaged records of the same sky areas obtained within the framework of RZF survey (curves 2). The scans are normalized to the level of the 3C84 signal. The curves are shown shifted along the vertical axis.

averaged real records of the RZF survey (curves 2) at 7.6 cm. All scans are normalized to the level of the 3C84 signal. The simulated scans based on the data of NVSS catalog and averaged real records were kindly provided by N. N. Bursov. Records are shifted with respect to each other along the vertical axis.

It is evident from a comparison of the curves shown in Fig. 5 that both models agree well with observational data, however, the small-scale structure of simulated scans

obtained using NVSS images is closer to that of real sky records. The simulated scans based on the NVSS catalog are smoother as compared to curves 1 and 2.

These differences are even more apparent in Fig. 6, which shows 10-minute portions of records. The differences can be explained by the fact that simulated scans based on the data of the NVSS catalog contain only the NVSS sources in the given declination band that have fluxes above a certain level. At the same time, the simulated scans constructed using NVSS images contain, in addition to NVSS sources, VLA detector noise convolved with the PB of RATAN-600, and the sources whose signals are at the detection level and close to the noise of the NVSS survey. Such sources could have escaped the NVSS catalog.

Note that the simulation of the RZF survey using the technique proposed by Bursov and Majorova [13] also has certain advantages. Thus the levels of the signals from the sources with known spectral indices are closer to the actual values for the model based on the NVSS catalog, because the fluxes of these sources were converted from $\lambda 21$ cm to $\lambda 7.6$ cm in accordance with their spectral indices.

Such an individual correction of source fluxes is very problematic to perform in the model proposed in this paper. The fluxes can be converted only in bulk for all sources in the record using the average spectral index.

3. SOME PROBLEMS THAT CAN BE SOLVED BY SIMULATING THE RZF SURVEY

Consider now the problems that can be solved with the simulated scans of the RFZ sky survey obtained.

Note that simulated scans based both on the data of the NVSS catalog and NVSS images have already been used to identify sources of the zenith-field sky survey and in the compilation of the RZF catalog [8]. The high degree of correlation between simulated and observed scans ($\sim 90\%$) allowed us to separate the contribution of discrete sources and background radiation, and to identify the sources in the survey records with the sources of the NVSS catalog. Simulated curves are especially valuable for detecting weak objects and for finding new objects undetected at decimeter-wave frequencies.

In this paper we also address a number of other problems. First, the analysis of simulated scans based on NVSS images allows us to estimate the accuracy of identification of sources and of the determination of their fluxes on sky-transit records. Second, simulated scans can be used to clean a real record from sources and estimate the minimum residual noise. Furthermore, it is of interest to estimate the spectral indices of the sources from the ratio of their signals on real and simulated scans and to compare their distribution with the distribution of spectral indices computed by Bursov et al. [8].

Before we start addressing these problems, let us list the main factors that may affect the accuracy of the simulation based on NVSS images. These factors include: the accuracy to which we know the power beam pattern of the

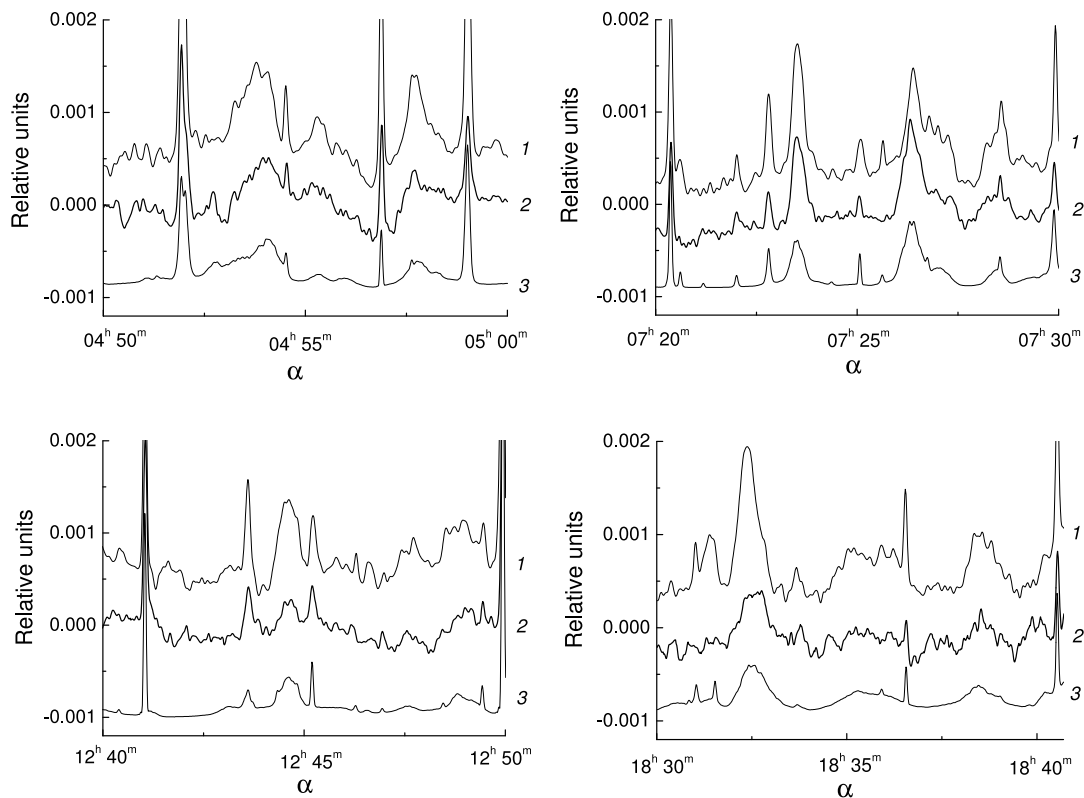


Fig. 6. Ten-minute portions of normalized simulated sky scans obtained using $4^\circ \times 4^\circ$ NVSS images (curves 1); the corresponding averaged records of the RZF survey (curves 2) at 7.6 cm, and simulated scans based on the data from the NVSS catalog [13].

radio telescope; the correctness of the source extraction on the simulated scans obtained, and the effect of the sizes of NVSS image areas on the results of simulation.

The values of the vertical PB are used to convert the antenna temperatures of the sources to the corresponding antenna temperatures for the central section of the survey and for the subsequent determination of the source fluxes. Majorova and Trushkin [12] and Majorova and Bursov [17] show that if the antenna is in good state, then the computed PB agrees with the experimental PB very accurately and therefore the errors due to the use of the computed PB are minimal and amount to mere $1 \div 3\%$.

Extraction of sources on simulated and real scans using the technique of Gauss analysis involves certain difficult aspects, especially when it comes to weak sources and sources with close right ascensions. We estimate the accuracy of the determination of the fluxes of the sources identified on records in Paragraph 6.

As for the effect of the size of the NVSS images on the results of simulation, our main task is to determine the maximum size of the area to minimize the simulation errors.

4. EFFECT OF THE SIZE OF NVSS IMAGES ON THE SIMULATION RESULTS

To perform the task mentioned above using simulated scans based on 7.6-cm NVSS images, we identify the sources of the NVSS catalog located within the $\pm 6'$ -band of the central declination of the survey. Like in the case of real records, we use the Gauss analysis [8, 16] to identify the sources, and control the declinations of the sources by the halfwidths of the Gaussians. To this end, we use the computed dependences of the halfwidth of the PB on its distance from the central section.

We identified a total of about 500 NVSS catalog sources with 21-cm fluxes $S > 2.7$ mJy. We determined the signal level for each of the sources identified both in relative units (in terms of the 3C84 signal level) and absolute units (mJy).

We construct the $\Delta\delta$ and $\Delta\alpha$ dependences of $S_m(0)/S_k$ for this sample of sources and determine the vertical PB of RATAN-600 and the dH dependence of the halfwidth of the power beam. Here S_k is the flux of the source according to the NVSS catalog; $S_m(0)$, the flux of the same source as inferred from the simulated scan and reduced to the central section of the survey ($\Delta\delta = 0$), and dH is the

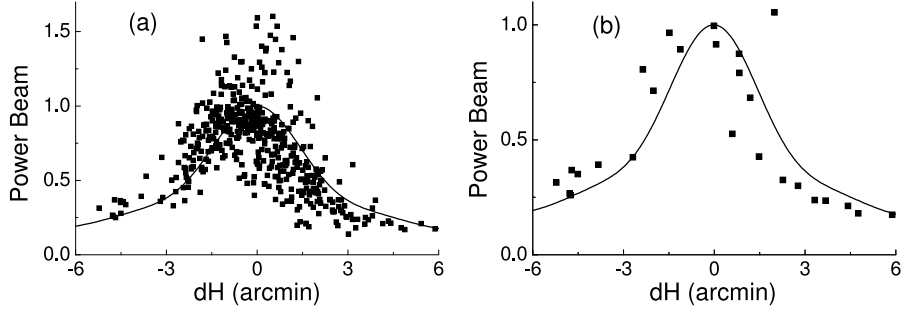


Fig. 7. Vertical PB constructed from sources extracted on simulated scans (filled squares) for the entire sample of sources ($S \geq 2.7$ mJy) (a) and from sources with fluxes $S \geq 200$ mJy—(b). Simulated scans were obtained using $4^\circ \times 4^\circ$ NVSS images. The solid lines indicate the vertical section of the computed PB at the wavelength of 7.6 cm after its convolving in each horizontal section with a Gaussian of width $\theta_{0.5} = 45''$.

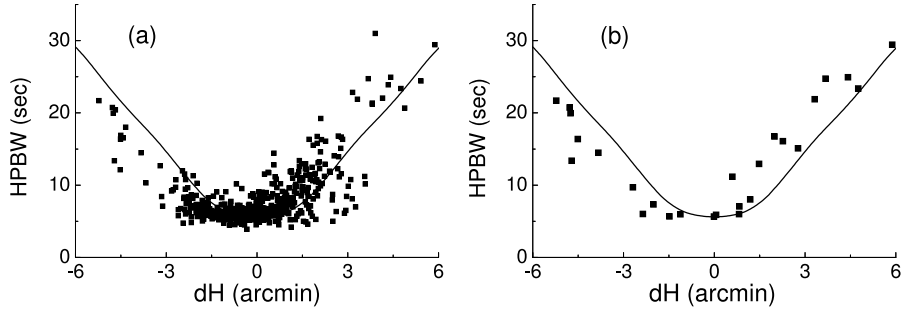


Fig. 8. The dH dependences of the halfwidth of PB constructed using the data for the sources extracted on simulated scans (filled squares) for the entire sample of sources ($S \geq 2.7$ mJy)—(a) and using sources with fluxes $S \geq 200$ mJy—(b). Simulated scans were obtained from $4^\circ \times 4^\circ$ NVSS images. The solid lines show the halfwidths of the computed PB at the wavelength of 7.6 cm convolved in each horizontal section with a Gaussian with a width of $\theta_{0.5} = 45''$.

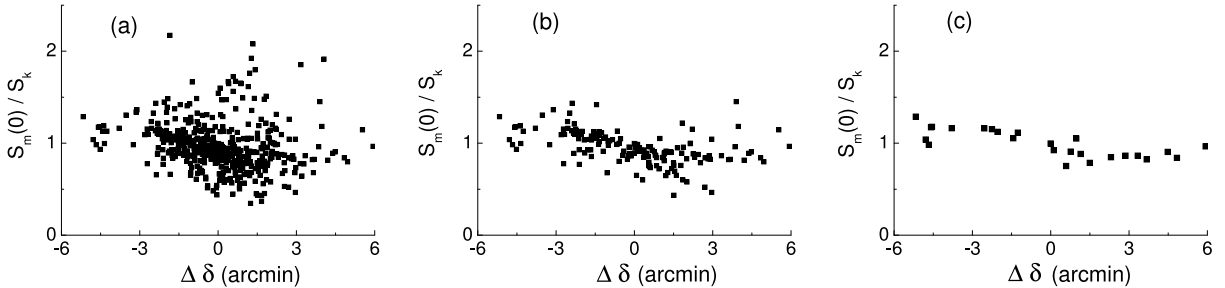


Fig. 9. The $\Delta\delta$ dependences of $S_m(0)/S_k$ constructed using the entire sample of sources extracted on simulated scans ($S \geq 2.7$ mJy) (a) and using sources with fluxes $S \geq 30$ mJy (b) and $S \geq 200$ mJy (c). The simulated scans were obtained from $4^\circ \times 4^\circ$ NVSS images.

elevation offset with respect to the central section of the PB.

$$S_m(0) = S_m(\Delta\delta)/F_r(dH), \quad (1)$$

where $S_m(\Delta\delta)$ is the flux of the source with the coordinates $(\delta_{ist}, \alpha_{ist})$ as inferred from the simulated scan; $F_r(dH)$, the vertical PB computed using computer codes in accordance with the technique described by Majorova [11], $\Delta\delta = \delta_{ist} - \delta_0$, $\Delta\alpha = \alpha_{ist} - \alpha_0$.

During the survey considered the central section of the PB passes through the central section of the survey, implying that $dH = \Delta\delta$.

The values F of the vertical PB of the radio telescope for various dH can be inferred from the following formula:

$$F(dH) = S_m(\Delta\delta)/S_k, \quad (2)$$

where $dH = \Delta\delta$, using the source fluxes inferred from simulated scans and the fluxes of the same sources listed in the NVSS catalog.

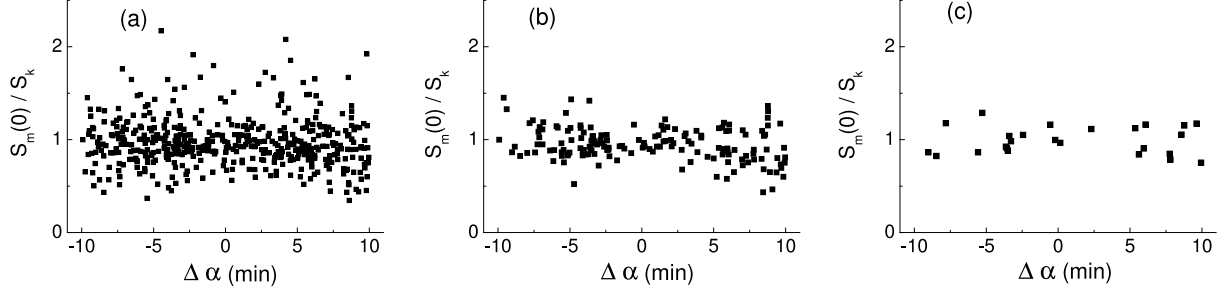


Fig. 10. The $\Delta\alpha$ dependences of $S_m(0)/S_k$ constructed using the entire sample of sources identified on simulated scans ($S \geq 2.7$ mJy) (a) and using sources with fluxes $S \geq 30$ mJy (b) and $S \geq 200$ mJy (c). The simulated scans were obtained from $4^\circ \times 4^\circ$ NVSS images.

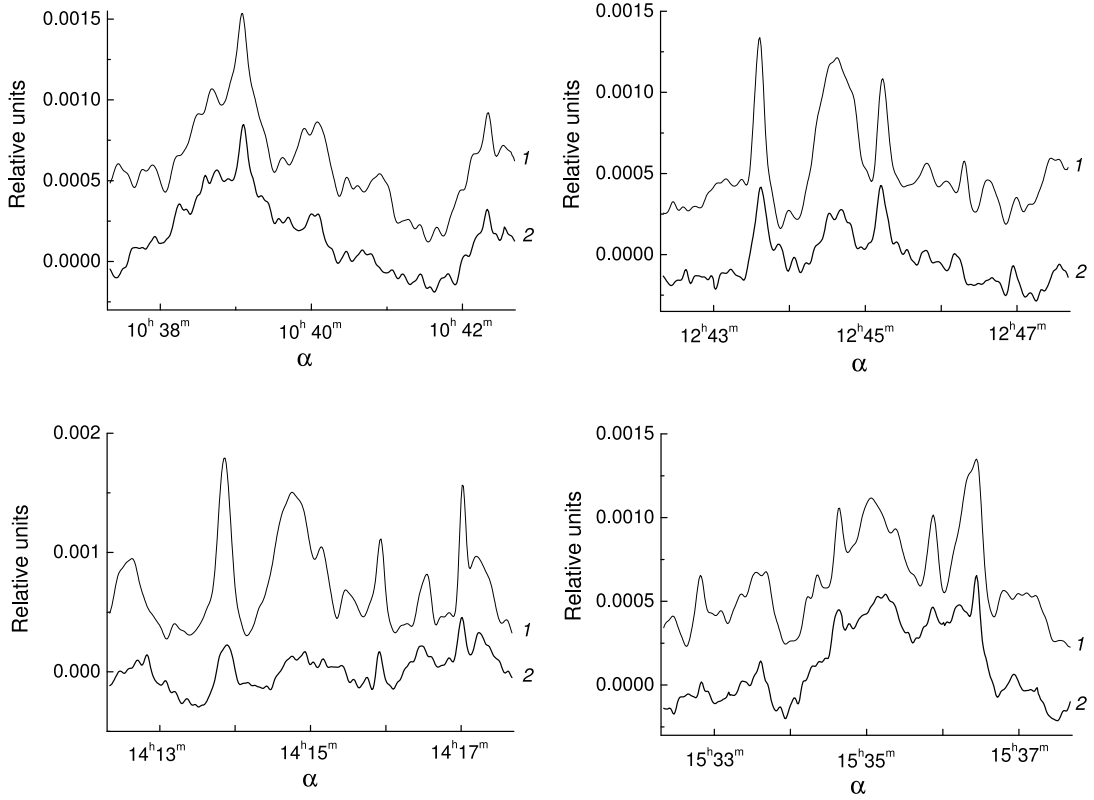


Fig. 11. Normalized five-minute simulated sky scans obtained using $1^\circ \times 1^\circ$ NVSS images (curves 1) and the corresponding averaged real records of the RFZ survey (curves 2) at the wavelength of 7.6 cm. All scans are normalized to the 384 signal level. The curves are shown shifted along the vertical axis.

The halfwidths of the power beams are equal to the halfwidths of the Gaussians fitted when identifying sources on simulated scans.

The filled squares in Figs. 7(a) and 8(a) show the vertical power beams and the dH dependences of HPBW constructed from the entire sample of sources identified on simulated scans, and Figs. 7(b) and 8(b) show the same power beams and dependences, but constructed from bright sources with fluxes $S \geq 200$ mJy. The solid lines show the vertical PB and the computed dH dependence of HPBW. Note that the two-dimensional power beams were

convolved with the images already convolved with the instrumental function of the VLA radio telescope, and therefore we convolved the computed PB of RATAN-600 in each of the horizontal sections with a Gaussian of halfwidth equal to $\theta_{0.5} = 45''$ (HPBW VLA [9]).

A sufficiently strong discrepancy between the power beams constructed from simulated scans and the computed curves is immediately apparent from Figs. 7 and 8. The pattern of the discrepancy does not depend on the brightness of the sources used to construct the dependences in question.

Figure 9 shows the $\Delta\delta$ dependences of $S_m(0)/S_k$ constructed for the entire sample of sources ($S \geq 2.7$ mJy) (a) and for the subsamples of sources with fluxes $S \geq 30$ mJy (b) and $S \geq 200$ mJy (c). All these dependences have a well-defined slope, indicating that the source fluxes inferred from simulated scans differ from the fluxes of the same sources listed in the NVSS catalog, and the discrepancy increases with the difference between the declinations of the source and of the central section of the survey. And, finally, the $\Delta\alpha$ dependences of $S_m(0)/S_k$ shown in Fig. 10 demonstrate that the discrepancy between $S_m(0)$ and S_k increases with increasing distance between the source and the scan center (or between the source and the centers of image areas Ihh20P40, Ihh00P40, and Ihh40P40). These features are especially apparent for the dependences based on the data for strong sources with fluxes $S \geq 30$ mJy and $S \geq 200$ mJy.

All these discrepancies are due to projection of the sky points (i.e. points of a sphere) onto the planes of the NVSS images. Condon et al. [9] give the formulas that relate celestial (α, δ) coordinates to pixel coordinates (x, y) of the image area:

$$x = x_0 - \cos\delta \sin(\alpha - \alpha_0)/\epsilon, \quad (3)$$

$$y = y_0 + [\sin\delta \sin\delta_0 - \cos\delta \sin\delta_0 \cos(\alpha - \alpha_0)]/\epsilon, \quad (4)$$

where $\epsilon = \pi/43200$ radian = $15''$, $x_0 = 512$, $y_0 = 513$.

It is evident from the above formulas that the farther is the source from the center of the sky area (α_0, δ_0), the greater is the error of its inferred position in the image plane. The difference between values of $\Delta\delta$ and $\Delta y = y_{ist} - y_0$ results in systematic errors in the inferred source fluxes reduced to the central section of the survey using the vertical power beam of the telescope. These errors, in turn, result in non-zero slopes of the dependences shown in Fig. 9, deviation of the simulated data points from the computed curves in Figs. 7 and 8, and in the increase of the scatter of data points toward the scan boundaries in Fig. 10.

The dependences shown in Fig. 10 can be used to select the maximum right-ascension sizes of image areas such that the $S_m(0)/S_k \sim 1$ condition is satisfied throughout the entire length of the simulated scan. This size is on the order of $d\alpha = \pm 2.5^m$ (or $\sim 1^\circ$). The declination size of the images, which is used in simulations, is close to its optimum value. Thus for the wavelength of $\lambda 7.6$ cm it is $d\delta = \pm 37'15''$.

Thus the simulated scans obtained by convolving 20-minute (in right ascension) sky areas of the NVSS survey with the two-dimensional PB of RATAN-600 are of great interest for the extraction of sources on real records of the zenith-field survey. The simulated and real scans are highly correlated and this correlation is especially useful for identifying weak sources. However, they are not suitable for quantitative estimates. To this end, the size of the image areas must be on the order of $1^\circ \times 1^\circ$ (about 5^m in terms of right ascension). Note that with such an image size both the number of images for the 7.6-cm wavelength

and the number of simulated scans increases by a factor of four. This was one of the reasons why we began our simulations with $4^\circ \times 4^\circ$ NVSS image areas.

5. SIMULATION OF THE ZENITH-FIELD SURVEY USING $1^\circ \times 1^\circ$ NVSS IMAGES

We simulated the zenith-field survey using $1^\circ \times 1^\circ$ NVSS images at the wavelength of 7.6 cm. We downloaded the images of the sky areas in FITS format from the site of SkyView [15] and converted them into the F format and then into 300×300 binary matrices. We then convolved the latter with the two-dimensional PB of RATAN-600 computed for $\lambda 7.6$ cm and having the same mesh size in α and δ as the images of the NVSS survey.

The centers of the image areas had the following coordinates: $\alpha_0 = H^h 5^m n$, $\delta_0 = +41^\circ 30' 45'' + \Delta$, where H are hours from 0 to 23, $n = 0, 1, 2, \dots, 11$, and Δ is the precession correction.

As a result, we obtained a total of 288 five-minute simulated scans. Figure 11 (curves 1) shows examples of such scans. The same figure shows the averaged five-minute records of sky transits obtained in the RFZ survey at the wavelength of 7.6 cm during the 1998–1999 period (curves 2). The simulated and real scans shown in the figures are normalized to the 384 signal level. The curves are shifted with respect to each other along the vertical axis.

As is evident from the figures, the simulated and observed scans are highly correlated. The correlation coefficient is ~ 0.95 , which is higher than the correlation coefficient between 20-minute simulated scans and the scans of the RFZ survey, and than the correlation coefficient between the simulated scans based on the data of the NVSS catalog and real records.

We use Gaussian analysis to identify the sources of the NVSS catalog on simulated scans; determine the amplitude (in relative and absolute units) and halfwidth of their signals. We then use the results obtained to construct the same dependences as those constructed for the sources identified on 20-minute simulated scans, namely: the $\Delta\delta$ and $\Delta\alpha$ dependences of $S_m(0)/S_k$, the dH dependence of HPBW, and the vertical PB of the radio telescope. We show the results in Figs. 12, 13, 14, and 15.

As is evident from the figures, the vertical PB and the dH dependence of HPBW constructed using five-minute simulated scans agrees well with the computed curves; the $\Delta\delta$ dependences of $S_m(0)/S_k$ have zero slopes, and the $\Delta\alpha$ dependences of $S_m(0)/S_k$ show a uniform scatter of data points along the entire scan length. This fact indicates that simulated scans contain no systematic errors and that they can be used to obtain qualitative estimates and not just to detect and identify the sources of the NVSS catalog on real scans.

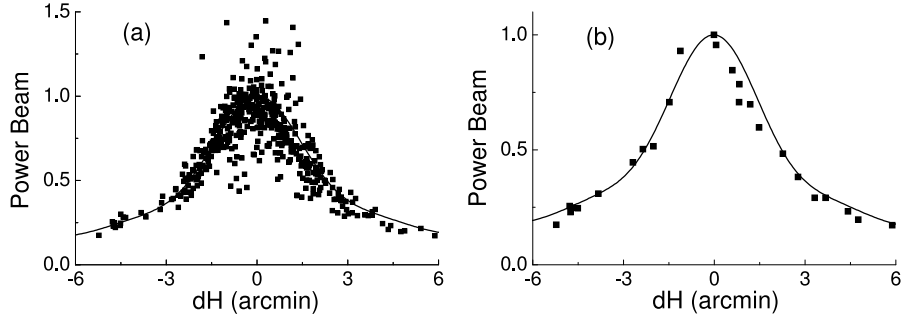


Fig. 12. Vertical PB constructed using the sources extracted on simulated scans (filled squares): for the entire sample of sources ($S \geq 2.7$ mJy) (a) and for sources with fluxes $S \geq 200$ mJy (b). The simulated scans were obtained from $1^\circ \times 1^\circ$ NVSS images. The solid lines show the vertical section of the computed PB at 7.6 cm after its convolving in each horizontal section with a Gaussian of size $\theta_{0.5} = 45''$.

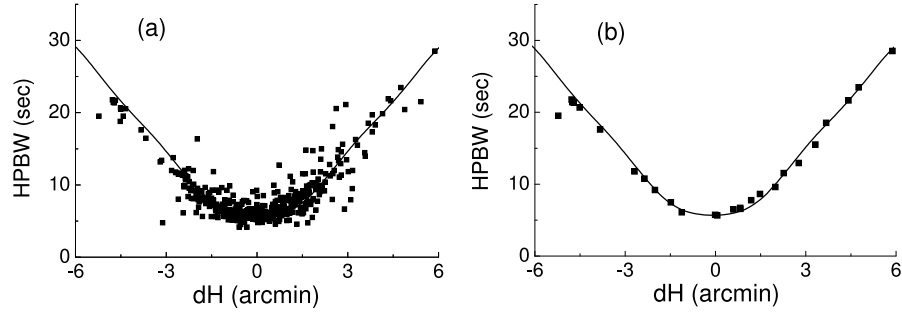


Fig. 13. The dH dependences of the halfwidth of the vertical PB constructed using the sources identified on simulated scans (filled squares): for the entire sample of sources ($S \geq 2.7$ mJy) (a) and for sources with fluxes $S \geq 200$ mJy (b). The simulated scans were obtained from $1^\circ \times 1^\circ$ NVSS images. The solid lines show the vertical section of the computed PB at 7.6 cm after its convolving in each horizontal section with a Gaussian of size $\theta_{0.5} = 45''$.

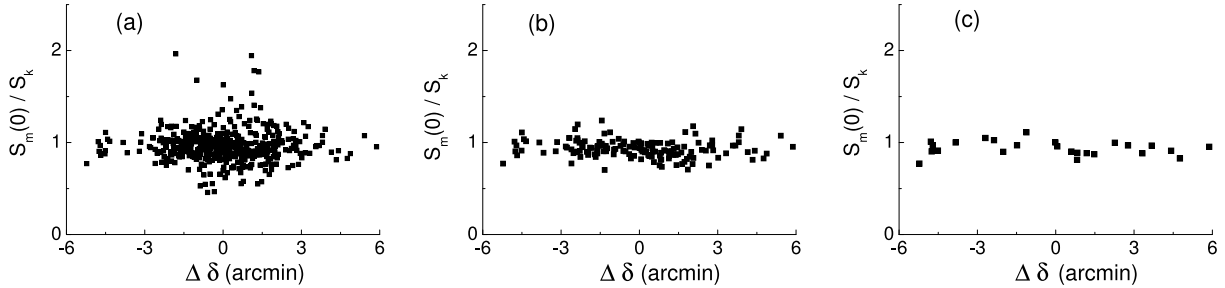


Fig. 14. The $\Delta \delta$ dependences of $S_m(0)/S_k$ constructed using the entire sample of sources identified on simulated scans ($S \geq 2.7$ mJy) (a) and using sources with fluxes $S \geq 30$ mJy (b) and $S \geq 200$ mJy (c). The simulated scans were obtained from $1^\circ \times 1^\circ$ NVSS images.

6. ESTIMATION OF THE ACCURACY OF THE INFERRED SOURCE FLUXES

Identification of NVSS sources on simulated scans obtained by convolving NVSS images with the power beam pattern of RATAN-600 and subsequent reduction of their fluxes to the central section of the survey must yield the fluxes given in the NVSS catalog. However, the dependences shown in Figs. 14(a,b,c) and 15(a,b,c) demon-

strate evident scatter of data points about $S_m(0)/S_k = 1.0$, and this scatter increases with decreasing source flux.

This is because as source fluxes decrease, source signals and the noise from background sources become close in magnitude, thereby making extraction of sources difficult both on simulated and real scans. Cases occur where sources blend together (are superimposed on each other). In some cases even strong sources are identified with insufficient confidence if they have close right ascensions, but are located at different distances from the central section

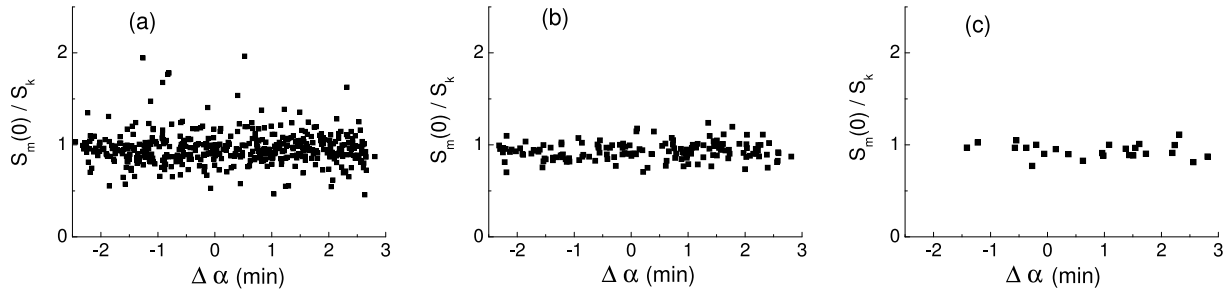


Fig. 15. The $\Delta\alpha$ dependences of $S_m(0)/S_k$ constructed using the entire sample of sources identified on simulated scans ($S \geq 2.7$ mJy) (a) and using sources with fluxes $S \geq 30$ mJy (b) and $S \geq 200$ mJy (c). The simulated scans were obtained from $1^\circ \times 1^\circ$ NVSS images.

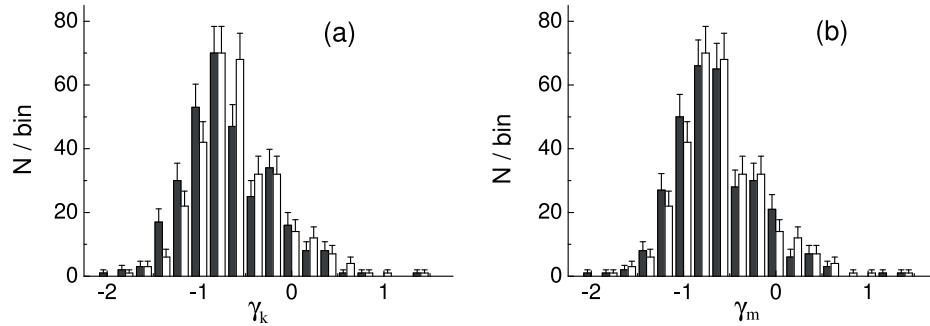


Fig. 16. Histograms of spectral indices obtained using the fluxes listed in the NVSS catalog, $\gamma = \ln(S_{7.6}/S_{21}^k)$ (a) (open bars), and using the fluxes inferred from simulated scans based on NVSS images, $\gamma = \ln(S_{7.6}/S_{21}^m)$ (b) (open bars). The histogram of spectral indices based on the data of the RZF catalog (filled bars) [8]. The histograms are based on a total sample of 317 sources with allowance for errors of inferred spectral indices.

of the survey. All the above effects result in the distortion of signals from sources and even in the appearance of false sources.

The errors of the inferred fluxes can be estimated using the resulting $\Delta\alpha$ dependences of $S_m(0)/S_k$. The standard error σ_S^m is equal to the standard deviation of $S_m(0)/S_k$ from its mean value averaged over the entire sample of the sources identified.

This error gives the lower limit for the error of the determination of fluxes of sources identified on real scans at $\lambda 7.6$ cm. Recall that the error of the inferred fluxes on real scans also includes the error of interpolation (extrapolation) of fluxes to the wavelength of 7.6 cm. Other error components should be of similar magnitude, because we use the same method to identify sources and use the same instrumental function of the radio telescope to convert the source fluxes to their values in the central section of the survey.

The standard error of the determination of the fluxes of the sources identified on simulated scans is: $\sigma_S^m = 0.20 \pm 0.01$ —for the entire sample of the sources considered with fluxes $S > 2.7$ mJy; $\sigma_S^m = 0.10 \pm 0.01$, for sources with $S > 30$ mJy and $\sigma_S^m = 0.08 \pm 0.01$, for sources with $S > 200$ mJy. (Here we give the source fluxes at $\lambda 21$ cm).

Let us now compare the errors of σ_S^m with the errors σ_S^r of the determination of the fluxes of sources identified in real records. The errors σ_S^r determined by Bursov et al. [8] and Majorova and Bursov [17] based on the entire sample of sources considered exceed σ_S^m by $20 \div 25\%$ ($\sigma_S^r = 0.24 \pm 0.03$ [17], $\sigma_S^r = 0.25$ [8]). For strong sources the error σ_S^r was equal to 0.15 ± 0.03 [8, 17].

As we pointed out above, such discrepancies between σ_S^m and σ_S^r are due primarily to errors of interpolation (extrapolation) of fluxes from $\lambda 21$ cm to $\lambda 7.6$ cm. However, a certain deviation of the real PB from the computed PB during the survey may also contribute to the above discrepancy.

7. DETERMINATION OF THE SPECTRAL INDICES OF THE SOURCES

The spectral index of a source can be computed as the logarithm of the $S_{7.6}/S_{21}^k$ ratio or the logarithm of the $S_{7.6}/S_{21}^m$ ratio, where $S_{7.6}$ is the flux of the source as inferred from the real averaged record of the RZF survey at $\lambda 7.6$ cm; S_{21}^k is the $\lambda 21$ cm flux of this source according to the data of the NVSS catalog, and S_{21}^m is the source flux in mJy as inferred from the simulated scan.

Given that we use the same technique to identify sources on real and simulated scans, and given the high degree of correlation between these scans, one may assume that the errors of the extraction of the same source should be the same for both scans. That is, we should either overestimate or underestimate the flux of a source when identifying it simultaneously in the simulated and real records. Thus the spectral indices computed by the formula $\gamma_m = \ln(S_{7.6}/S_{21}^m)$ may prove to be even more accurate than those inferred from the data of the NVSS catalog ($\gamma_k = \ln(S_{7.6}/S_{21}^k)$). This is true if the computed and real power beams of the radio telescope agree well with each other.

To compare the spectral indices of the sources obtained using different methods, we identify on the averaged 7.6-cm records of the RZF survey the sources of the NVSS catalog within the $\pm 6'$ band of the central section of the RZF survey. We identified a total of about 500 NVSS-catalog sources on the 24-hour record of the sky scan, determine the spectral indices γ_k and γ_m for each of these sources, and compare them to the spectral indices obtained by Bursov et al. [8]. For a more correct comparison, we used only the sample of 317 sources in common with the RFZ catalog.

The open bars in Fig. 16 show the histograms of the distribution of spectral indices obtained using the fluxes listed in the NVSS catalog, $\gamma_k = \ln(S_{7.6}/S_{21}^k)$ (a) and the distribution of spectral indices computed using the fluxes obtained from simulated scans $\gamma_m = \ln(S_{7.6}/S_{21}^m)$ (b). The histograms are based on the sample of 317 sources that we identified on simulated and real scans. The filled bars in the same figure show the histograms of the spectral indices of the same sample of sources based on the data of the RZF catalog [8]. These histograms were constructed with allowance made for the errors of the determination of spectral indices.

As is evident from the figures shown, the histogram of the spectral indices γ_m computed using the fluxes inferred from simulated scans proves to be closer to the distribution of spectral indices according to the data of the RZF catalog for the source sample considered. Given the confidence interval, they can be considered to be virtually identical.

It follows from this that given the real records and the corresponding simulated scans obtained using NVSS images, one can infer the spectral indices of the sources from the ratio of their signals in the scans considered. The real and simulated scans must be normalized prior to that. Such a procedure is very easy and convenient to perform for sources whose spectral indices are unknown.

8. ESTIMATE OF RESIDUAL NOISE ON REAL RECORDS USING SIMULATED SCANS

We use the simulated scans based on NVSS images to clean the real records from discrete sources. To this end, we “join” the normalized five-minute scans into a single

24-hour scan and convert it into a 7.6-cm wavelength scan in accordance with the average spectral index.

As we pointed out above, in this method it is hardly possible to correct the signal from each source in accordance with its own spectral index even if the spectral index is known, and therefore we used for our conversion the spectral indices close to those of the sources with normal nonthermal spectra, which lie in the $\gamma = 0.78 \pm 0.02$ interval. We chose the spectral index so as to minimize the standard error of the deviation of the simulated record corrected for the spectral index from the real record. We used trimmed records $0^h \leq \alpha < 20^h$ (with the Galactic plane excluded) to estimate the magnitude of residual noise.

The standard error of residual noise at 7.6 cm was equal to $\sigma = 7.6 \pm 0.9$ mJy. This residual noise includes the noise due to unresolved sources; radiometer noise; atmospheric noise, and residual signals from the sources whose spectral indices differ from the average spectral index used to convert the source fluxes.

Subtraction of the background inferred with a $30''$ smoothing window (hereafter referred to as the thirty-second background) partially eliminates atmospheric noise and the noise from the sources located outside the $\Delta\delta = 41^\circ 30' 42'' \pm 6'$ band. This procedure reduces σ of residual noise down to 4.6 ± 0.6 mJy. Note, for comparison, that the magnitude of residual noise after we subtract from the real averaged record the simulated scan obtained from the data of the NVSS catalog and then the thirty-second noise, is equal to $\sigma = 5.9 \pm 0.6$ mJy. This means that cleaning real records using simulated scans obtained by applying two different methods yields similar results.

Figure 17(a) shows the residual noise on a real averaged record of the RZF survey after subtracting from it the simulated scan based on NVSS images and corrected for the average spectral index. Figure 17(b) shows the residual noise obtained after further subtraction of the background computed with a $30''$ smoothing window from the difference of the real and simulated scans.

As is evident from the figures, the records still contain signals from the sources whose spectral indices differ from the average spectral index. After eliminating such signals (they can be easily seen in the records) the standard deviation σ of the residual noise becomes equal to about 1 mJy. Figure 17(c) shows the record of the residual noise. Note that the standard error of the same portion of the uncleaned real record ($0^h \leq \alpha < 20^h$) is equal to 19 ± 3 mJy. We did not take the 3C84 signal into account when estimating σ . Thus cleaning of records using simulated scans reduces the residual noise of a real record by more than one order of magnitude.

Note that records can be cleaned even without the use of simulated scans, simply by “cutting” the sources on records in accordance with their coordinates. However, such a cleaning procedure is very time consuming and sometimes ambiguous, because the transit curves obtained in RATAN-600 surveys are superpositions of source signals convolved with the PB at different declinations. The proposed method allows easy elimination of most of the

point sources within the given declination band and with fluxes greater than 3 mJy ($> 3\sigma$). More refined methods are required for a more in-depth cleaning, and we do not describe them here, because they are a subject of a separate paper.

9. CONCLUSIONS

We propose and develop a method for the simulation of a deep multi-frequency zenith-field sky survey by convolving NVSS images with two-dimensional power beams of RATAN-600.

We perform simulations at 1.0, 2.7, 3.9, 7.6, 13, 31, and 49 cm in the central band of the survey. We obtained 24-hour simulated scans of the sky transit across the power beam pattern of the telescope at each of the wavelengths listed above and compared the simulated scans with real records and with the simulated scans based on the data of the NVSS catalog [13].

We analyze the effect of the size of NVSS-image areas on the results of simulations at 7.6 cm. We show that simulated scans based on $4^\circ \times 4^\circ$ (20^m in right ascension) NVSS image areas are highly correlated (with a correlation coefficient of $\sim 90\%$) with real scans and can therefore be used to identify and extract weak sources in the records of the RZF survey. However, for quantitative estimates the size of NVSS image areas should be reduced down to $1^\circ \times 1^\circ$ (5^m in right ascension).

We obtained a total of 288 five-minute simulated scans of sky transits at the wavelength of 7.6 cm by convolving $1^\circ \times 1^\circ$ NVSS images with the PB of RATAN-600, and then “joined” them into a single 24-hour scan. We identified a total of about 500 NVSS-catalog sources simultaneously in simulated scans and real averaged records of the RZF survey within the $\pm 6'$ band of the central section of the survey and estimated their fluxes.

The data obtained allowed us to estimate the accuracy of the determination of source fluxes on simulated scans. The standard error of the determination of source fluxes on simulated scans is $\sigma_S^m = 0.20 \pm 0.01$ for the entire sample of sources considered ($S > 2.7$ mJy). This error is $20 \div 25\%$ lower than the standard error for real records [8, 17]. The standard error is $\sigma_S^m = 0.10 \pm 0.01$ for sources with fluxes exceeding 30 mJy. The standard errors σ_S^m obtained can be viewed as a lower limit for the errors of the determination of source fluxes on real scans at $\lambda 7.6$ cm.

We derived the distributions of spectral indices of the sources by identifying sources on real and simulated scans. To compute the spectral indices, we used the source fluxes listed in the NVSS catalog and the source fluxes inferred from real and simulated scans. We compared the distributions of spectral indices obtained using different methods with the distribution of spectral indices based on the data of the RZF catalog for the common sample of 317 sources. We show that the distribution of spectral indices computed as the logarithm of the ratio of the fluxes of sources identified on real and simulated scans agrees within the quoted errors with the distribution of spectral indices in-

ferred from the data of the RZF survey of the same sample of sources.

We use the simulated scans obtained to clean the real 20-hour record of the RZF survey. After the subtraction of the thirty-second noise and elimination of residual signals of the sources whose spectral indices differ from the mean spectral indices the standard deviation σ of residual noise was equal to ~ 1 mJy at 7.6 cm. This procedure reduced the noise of the initial record of the RZF survey by more than one order of magnitude.

Acknowledgements. I am grateful to Yu. N. Parijskij for his support of the work and discussion of the results, N. N. Bursov for sharing the data of the RZF survey and simulated scans based on the NVSS catalog.

This work was supported in part by the Russian Foundation for Basic Research (grant no. 05-02-17521) and the Program for the Support of Leading Scientific Schools of the President of the Russian Academy of Sciences (the “School of S. E. Khaikin”).

References

- [1] Yu.N.Parijskij and D.V.Korol'kov, *Itogi Nauki i Tekhniki. Astrofiz. Kosmicheskaya Fiz. Edited by R.A.Sunyaev. Seriya Astronomiya* (VINITI, Goskomitet po Nauke i Tekhnike, Moscow, 1986) **31**, 73 (1986).
- [2] Yu. N. Parijskij, N. N. Bursov, N. M. Lipovka, et al., *Astron. and Astrophys. Suppl.* **87**, 1 (1991).
- [3] Yu. N. Parijskij, N. N. Bursov, N. M. Lipovka, et al., *Astron. and Astrophys. Suppl.* **96**, 583 (1992).
- [4] *Catalog of Radio Sources of the Zelenchuk Sky Survey in the Declination Interval $0^\circ - 14^\circ$* , Edited by M. G. Larionov (Izdatel'stvo Moskovskogo Universiteta, 1989).
- [5] V. R. Amirkhanyan, A. G. Gorshkov, and A. V. Ipatov, *Soobshch. Spets. Astrofiz. Obs.* **58**, 41 (1988).
- [6] V. R. Amirkhanyan, A. G. Gorshkov, A. A. Kapustin, et al., *Pis'ma Astron. Zhurn.* **18**, 396 (1992).
- [7] M. G. Mingaliev, O. V. Verkhodanov, and A. R. Khabrakhmanov, *Pis'ma Astron. Zhurn.* **17**, 787 (1991).
- [8] N. N. Bursov, Yu. N. Parijskij, E. K. Majorova, et al., *Astron. Zhurn.* **84**, 227 (2007).
- [9] J. J. Condon, W. D. Cotton, E. W. Greisen, et al., *Astronom. J.* **115**, 1693 (1998)
- [10] R. L. White, R. H. Becker, D. J. Helfand, and M. D. Gregg, *Astrophys.J.* **475**, 479 (1997).
- [11] E. K. Majorova, *Bull. Spec. Astrophys. Obs.* **53**, 78 (2002).
- [12] E. K. Majorova and S. A. Trushkin, *Bull. Spec. Astrophys. Obs.* **54**, 89 (2002).
- [13] N. N. Bursov and E.K.Majorova, in *Abstracts of Papers. Russian Conference Dedicated to the Memory of A. A. Pistel'kors "Radio telescopes RT-2002", Pushchino, October 9–11, 2002*, 26, (2002).
- [14] J. J. Condon, W. D. Cotton, E. W. Greisen, et al., <http://www.cv.nrao.edu/nvss/>, <http://ftp.cv.nrao.edu/fits/os-support/unix/xfitsview/>.
- [15] SkyView, <http://skyview.gsfc.nasa.gov/cgi-bin/skvbasic.pl>.
- [16] N. N. Bursov, Candidate's Dissertation in Physics and Mathematics (Special Astrophysical Observatory, Russian Academy of Sciences, Nizhnii Arkhyz, 2003).
- [17] E. K. Majorova and N. N. Bursov, *Astrophys. Bull.* **62**, 398 (2007).

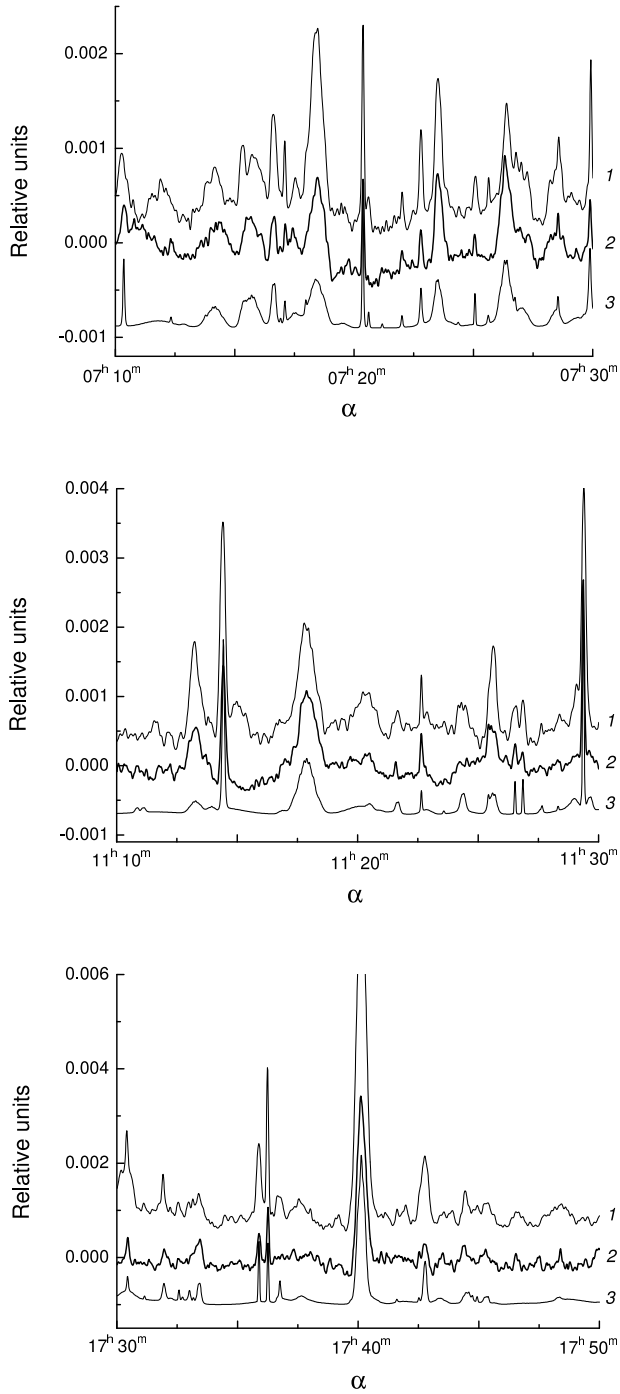


Fig. 5. Normalized 20-minute simulated sky scans obtained using $4^\circ \times 4^\circ$ NVSS images (curves 1); the corresponding real records of the RZF survey (curves 2) at $\lambda 7.6$, and simulated scans based on the data of NVSS catalog [13] (curves 3). All scans are normalized to the 3C84 signal level. The curves are shown shifted with respect to each other along the vertical axis.

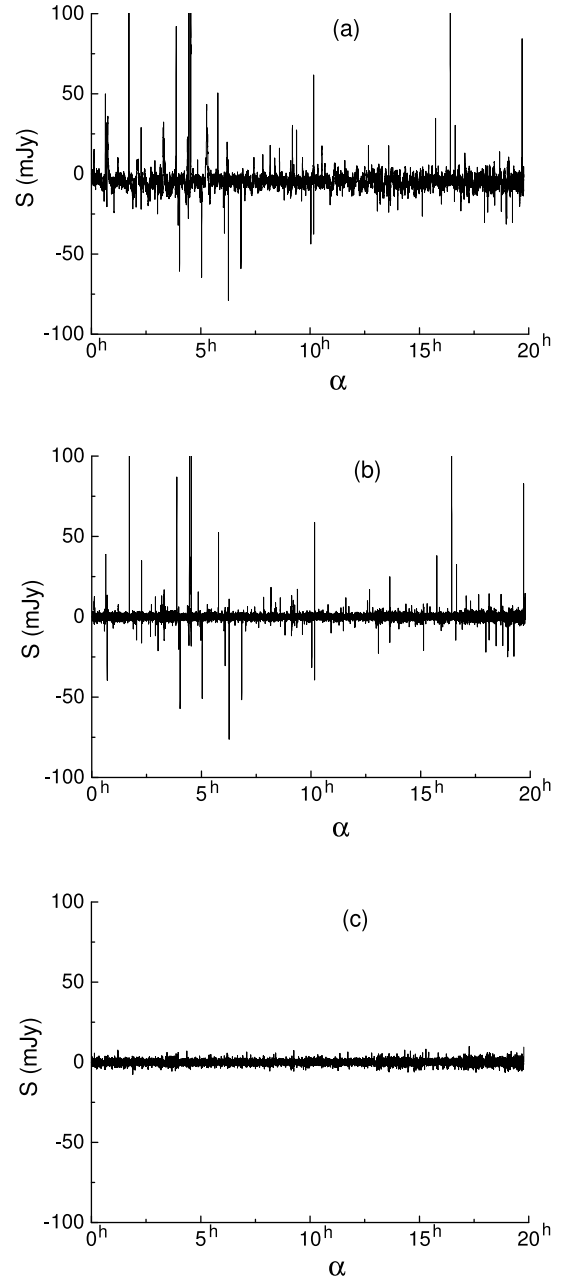


Fig. 17. Residual noise on a real averaged record of the RZF survey after subtracting the simulated scan obtained using NVSS images (a); residual noise after subtracting the background obtained with a 30^s smoothing window from the difference of the real and simulated scans (b), and residual noise after subtracting the sources whose spectral indices differ from the average spectral index (c).